ARTICLE NO. 79-0252R

Electron Attachment at High Temperatures

Ven H. Shui,* Param I. Singh,* Bennett Kivel,* and Ellen R. Bressel†
Avco Everett Research Laboratory, Inc., Everett, Mass.

Electron attachment measurements were carried out in the Chemical Modeling Experimental Facility (CMEF) over the temperature and pressure ranges 3500-500 K and 70-10 Torr. The CMEF consists of a jet of partially ionized hot air whose temperature is about 3800 K at the nozzle. The attachers studied include SF_6, oxides of boron, rhenium, and tungsten; perrhenic acid; SO_2F_2; CF_3Br; CCl_4; C_7F_{14}; HCl; HI; $ClC_6H_4CF_3$; $ClC_6H_3(NO_2)CF_3$; CrO_2Cl_2; teflon monomer and polymer; WF_6; MoF_6; and ReF_6. Attachment data and detailed analyses indicate that many attachers have large attachment-rate constants ($\gtrsim 10^{-8}$ cm^3/s). At high temperatures, however, attachment performance is also critically dependent on the stability of the negative ion, which in turn is a sensitive function of the electron affinity. In particular, we find that 1) attachment performance of SF_6 degrades at high temperatures, 2) tungsten oxides, WF_6, MoF_6, and ReF_6 perform better than SF_6 at high temperatures, 3) the electron affinity for tungsten oxides is about 3.6 eV while WF_6, the best high-temperature electron attacher of those studied, has an electron affinity of $\approx$5.5 eV, and 4) hydrogen, when present in high enough concentrations, degrades the high-temperature attachment performance of SF_6 and WF_6.

I. Introduction

THE process of electron attachment to molecules has numerous practical applications. Most obvious from the point of view of aeronautics and astronautics is RF blackout alleviation in re-entry flight. It is also an important process for the chemical kinetics of certain new lasers, and for altering the radar signature of a re-entry-vehicle wake or the signature of a rocket-exhaust plume. Some of the general principles presented in this paper concerning electron attachment may even have applicability to magnetohydrodynamic power generation where the aim is to keep electron attachment at a minimum.

Sulfur hexaflouride has been the most commonly used molecule for electron attachment because of its large rate constant or cross-section for this process. For example, Fehsenfeld[1] reported a measured attachment-rate constant of 2.2×10^{-7} cm^3/s, independent of temperature in the temperature range 293-523 K. However, a large attachment-rate constant is only one of several important properties required for a good electron attacher. At high temperatures, decomposition of the molecule becomes more rapid[2] and the stability of the negative ion formed, which is roughly proportional to exp (EA/kT) where EA is the electron affinity, decreases rapidly. Thus, other molecules may have better electron-attachment properties than SF_6. Some of these molecules reported in the literature are tungsten oxides,[3] Freon E-3,[4] and rhenium oxides.[5]

We have carried out a study of the electron attachment performance of a large number of candidate molecules including SF_6, oxides of boron, rhenium and tungsten, perrhenic acid, SO_2F_2, CF_3Br, CCl_4, C_7F_{14}, HCl, HI, $ClC_6H_4CF_3$, $ClC_6H_3(NO_2)CF_3$, CrO_2Cl_2, teflon monomer and polymer, WF_6, MoF_6, and ReF_6. Measurements of electron attachment were carried out in the Chemical Modeling Experimental Facility (CMEF), the temperature and pressure ranges covered in the experiments being 3500-500 K and 70-10 Torr, respectively. Detailed analyses of the attachment performance have also been carried out for a number of the candidate molecules in order to understand and explain the data.

The experimental facility and major diagnostic instruments for making electron attachment measurements are described in the following section. Our experimental data are summarized in Sec. III. In Sec. IV we present our general analysis as well as some detailed analyses for the attachment performance of several candidate molecules, and Sec. V contains our concluding discussion.

II. Experimental Facility

The chief experimental tool for the present study was the Chemical Modeling Experimental Facility. A brief description of the CMEF and some of its early applications in re-entry-wake studies have been presented before.[6] A schematic diagram of the CMEF is shown in Fig. 1. An RF induction arc is used to heat a jet of air which becomes partially ionized and passes through a 1-in.-diam nozzle into an 8-ft diam by 22-ft long tank where a variety of tests and measurements can be carried out. The jet is subsonic and its turbulent growth is accommodated by entraining pure air which flows into the tank through side-wall injection rings as shown in Fig. 1. Figure 2 shows the measured centerline temperature profile in the CMEF at the typical operating conditions of 1 g/s initial jet-mass flux and 20-Torr ambient pressure.

A. Injection of Attaching Molecules

The bulk of attachers tested were either gases at STP or had sufficient vapor pressure to be injected as gases into the 20-Torr ambient pressure of the arc-heated jet environment. Injection was coaxial along the jet centerline with the species being transported either through a water-cooled stainless-steel tube or through ceramic tubes (slip-cast zirconia). Mass fluxes were measured using flow meters or sonic-choked orifices. The following species were injected in this manner: SF_6, SO_2F_2, CF_3Br, CCl_4, C_7F_{14}, HCl, HI, $ClC_6H_4CF_3$, $ClC_6H_3(NO_2)CF_3$, CrO_2Cl_2, C_2F_2 stabilized monomer, WF_6, MoF_6, and ReF_6. The mass flux and momentum of the injected species are much smaller than the arc-jet values and large-scale mixing of the two streams is by turbulent diffusion.

Received Nov. 2, 1978, presented as Paper 79-0252 at the 17th Aerospace Sciences Meeting, New Orleans, La., Jan. 15-17, 1979; revision received April 20, 1979.

Index categories: Plasma Dynamics and MHD; Reactive Flows.

*Principal Research Scientist. Member AIAA.

†Vice President.

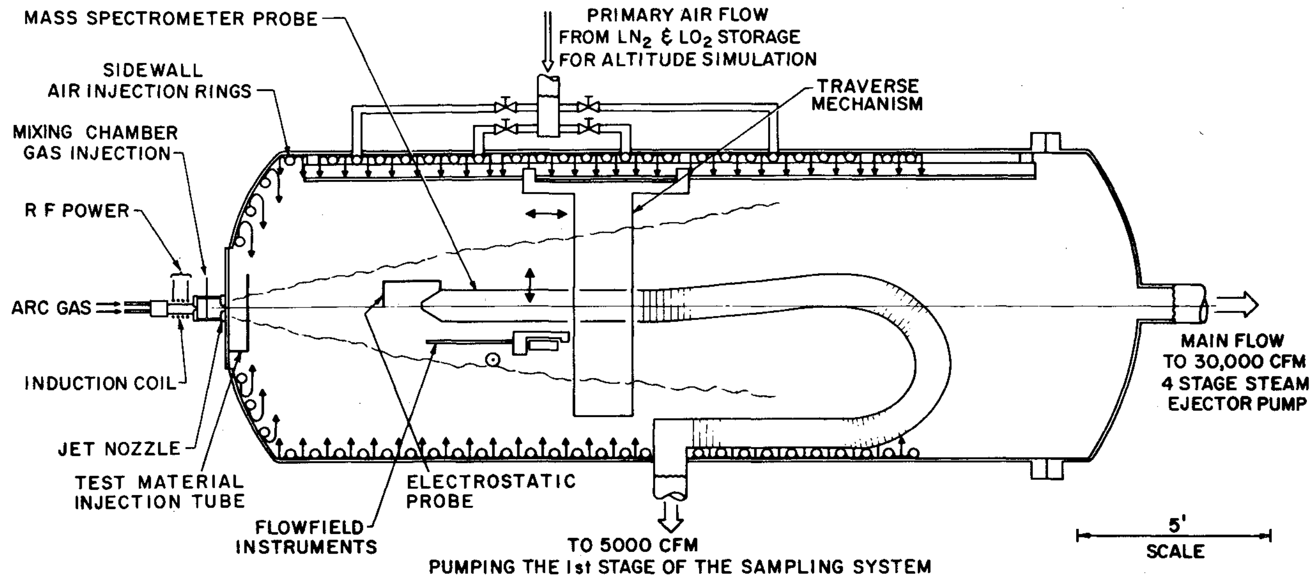

Fig. 1 Scale drawing of Chemical Modeling Experimental Facility (CMEF).

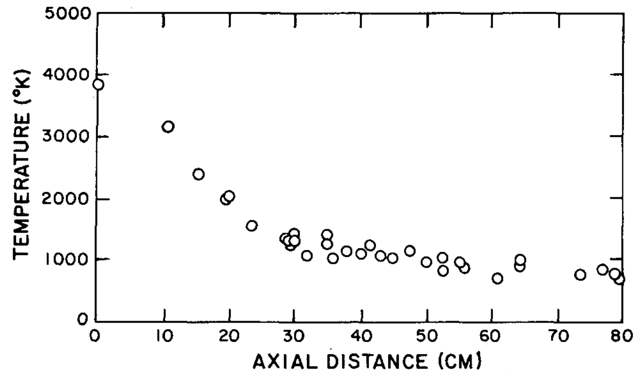

Fig. 2 Measured CMEF turbulent air-jet centerline temperature. Ambient pressure = 20 Torr, jet-mass flux = 1 g/s.

The oxides of tungsten, boron, and rhenium were seeded into the turbulent jet by ablating weighed tubes of tungsten, boron nitride, and rhenium. The determination of mass-loss rate was simple for boron nitride, where the difference in weight before and after the experiment was corrected only for the percent boron content of the rod. For tungsten and rhenium, this procedure was complicated by the coating of the samples with oxides of these metals. The mass-loss rate was determined by chemically removing these oxides without removing virgin metal and correcting for the tungsten content in the oxides.

Perrhenic acid, $Re_2O_7 \cdot 2H_2O$, was injected as a liquid jet perpendicular to the arc-jet axis. Calculations showed that the liquid would be completely vaporized in the vicinity of the jet axis and this was confirmed by visual observation.

B. Electrostatic Probe and Determination of Attachment

The major diagnostic instrument used in the CMEF for the electron-attachment experiment is the electrostatic probe. Cylindrical probes of 0.002-in. and 0.010-in. diameters were used in the CMEF experiments; probe length was generally between 6 mm and 8 mm. Theories are available for determining positive-ion number densities from the probe data; for example, Mott-Smith and Langmuir[7] and Laframboise[8] for the free-molecule limit; Zakharova, Kagan, Mustafin and Perel[9] and Kiel[10] for the continuum limit; and Scharfman and Taylor[11,12] for calculating the convection current under various conditions. The positive-ion number density n_+ calculated from measured quantities by using results published in these papers are shown in Fig. 3 for 20-Torr pressure, where the positive-ion number density is plotted vs the axial distance from the jet exit. The solid line in the figure is the result of calculation using the AERL 2D computer code, assuming an initial ion density to be given by the equilibrium value at the jet-exit conditions. Three sets of experimental data are shown in the figure. The symbols △ and ▲ represent data obtained with the 0.002-in. diam probe but interpreted with the free-molecule and the continuum limits, respectively. The symbol ● represents data from the 0.010-in. diam probe, interpreted with the continuum limit. Mean free-path calculations for the CMEF conditions indicate that the 0.010-in. diam probe satifies the continuum limit whereas the 0.002-in. diam probe is in the transition regime.

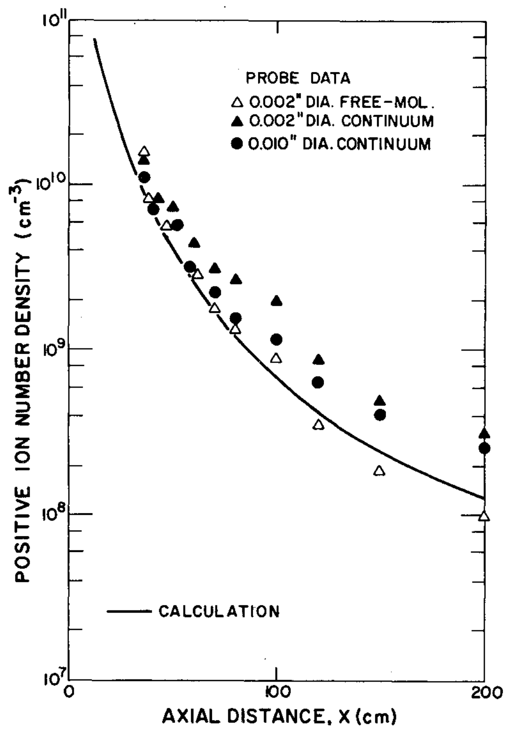

Fig. 3 Plot of positive-ion number density vs axial distance for the CMEF turbulent jet at 20-Torr pressure.

Although the probe data provided useful information on the positive-ion densities, the primary application of the

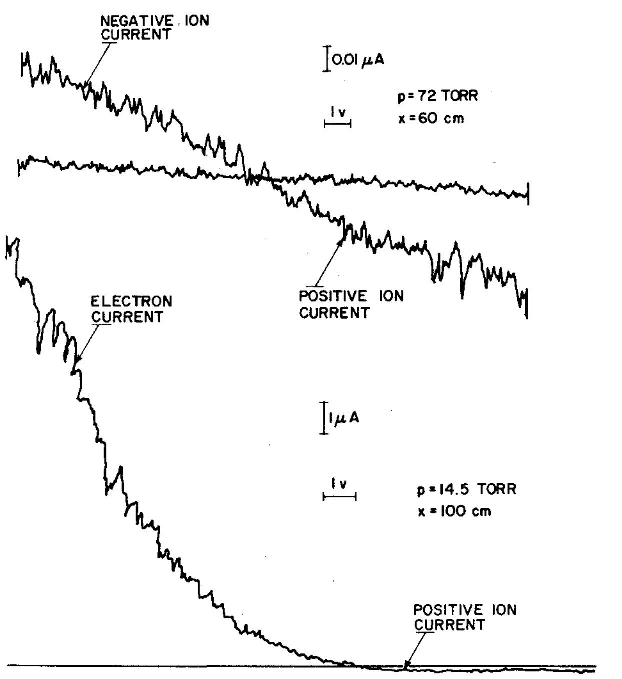

Fig. 4 Electrostatic-probe current-voltage traces obtained in CMEF air jets.

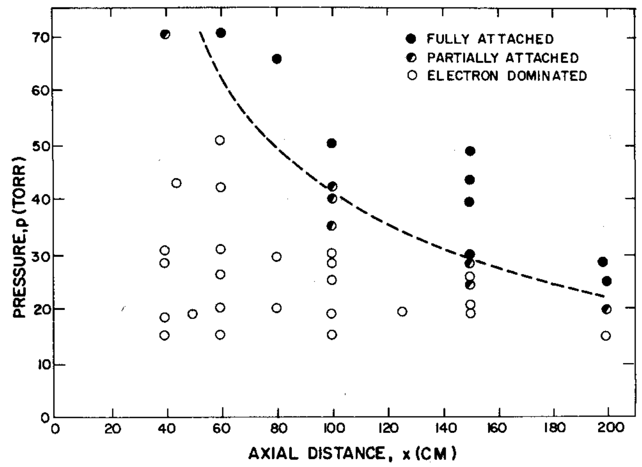

Fig. 5 The electrostatic-probe-generated map of the turbulent jet indicates which regions are suitable for attachment experiments.

electrostatic probes in the present experiments was the determination of attachment in the plasma. When there are no negative ions in the plasma and all positive ions are singly charged, the number densities for electrons and for positive ions are equal. The electron current collected by the probe when it is positively biased will be much larger than the positive-ion current collected by the probe when it is negatively biased. This is a result of the positive-ion mass being much larger than the electron mass, and the difference in currents generally exceeds a factor of 100. On the other hand, when all the electrons are attached to form negative ions, the difference in the positive- and negative-ion currents will be very small, because they have similar masses.

This means that the current-voltage characteristics will be so different for these two cases described above that they may be used for the unambiguous determination of attachment in the jet. This is illustrated by Fig. 4, which shows two different records of the current-voltage characteristics. The top part of Fig. 4, recorded for $p = 72$ Torr and $x = 60$ cm, shows almost equal positive and negative currents, indicating that the turbulent air jet is fully attached. The lower part of Fig. 4, recorded for $p = 14.5$ Torr and $x = 100$ cm, shows much larger negative current than positive current, indicating that the jet is still electron-dominated.

Figure 5 presents a map of the natural attachment in the CMEF jet using electrostatic probe results to indicate, as a function of ambient pressure, which regions of the jet are electron-dominated, i.e., suitable for attachment experiments. Three symbols are shown in the figure indicating electron-dominated, partially attached, and fully attached regions of the jet. The dashed curve indicates a rough boundary between the electron-dominated region (to the lower left) and the attached region (to the upper right). As the ambient pressure is increased, the axial distance at which attachment occurs decreases. For example, at 50-Torr ambient pressure, attachment experiments can be performed only at distances up to about 60 cm, at which point the air jet shows significant attachment. At 20-Torr ambient pressure, experiments can be performed to distances greater than 150 cm. These experimental results are in good agreement with calculations which solve conservation equations for a jet including appropriate chemical reactions. The attachment of electrons by molecules injected into the jet can be investigated in a similar manner.

We note that this method of determining electron attachment is based on the relative magnitudes of the measured positive and negative probe currents, and does not depend on any calculated values of electron, positive-ion, or negative-ion densities. The determination of electron attachment is valid in either continuum or free-molecule regime, with or without convection, and regardless of the sheath thickness. Furthermore, as will be indicated by Eqs. (4) and (7) in Sec. IV, the exact determination of when "full" attachment occurs is not needed to obtain reasonably accurate values of the important attacher properties such as attachment rate and electron affinity.

Table 1 Summary of electrostatic-probe data[a]

Attacher	Mass flux (g/s)	Electrostatic-probe data[b]
SF_6	4×10^{-3}	30P, 45F
SF_6	3×10^{-2}	25P, 30F
SF_6[c]	5×10^{-4}	30P, 45F
Boron oxides[d]	1×10^{-4}	70N, 80P, 140P
Boron oxides[d]	7×10^{-3}	80F
Rhenium oxides[d]	8×10^{-5}	90P, 150P
Rhenium oxides[d]	2×10^{-3}	40F
Tungsten oxides[d]	8×10^{-4}	45P, 55F
Tungsten oxides[d]	1.2×10^{-3}	24N, 29F
$Re_2O_7\cdot2H_2O$[c]	0.1	100P, 200F
SO_2F_2[c]	2×10^{-3}	40N, 60F
SO_2F_2[c]	5×10^{-2}	25N, 40F
CF_3Br[c]	2×10^{-2}	30P, 45F
HCl[c]	0.1	40N, 80F
HI	0.13	55N
$ClC_6H_4CF_3$	5×10^{-3}	55N, 65F
$ClC_6H_3(NO_2)CF_3$	3.5×10^{-4}	65N
CrO_2Cl_2	2×10^{-2}	55N
C_2F_4 monomer	1×10^{-2}	75N
C_2F_4 polymer	1.5×10^{-3}	35P, 55P, 65F
WF_6	2.6×10^{-5}	35N, 40F
WF_6	2.6×10^{-4}	16N, 20F
WF_6[c]	2.6×10^{-4}	23N, 28F
MoF_6	2.2×10^{-4}	18N, 28F
MoF_6	2.2×10^{-3}	18N, 23F
ReF_6	2.3×10^{-4}	53N, 58P, 63F
ReF_6	2.1×10^{-3}	28N, 33F

[a] Data at an ambient pressure of 20 Torr with injection at 11 cm from jet exit ($T > 3000$ K.) [b] N = no attachment ($I_-/I_+ > 50$), P = partial attachment ($50 > I_-/I_+ > 5$). F = full attachment ($I_-/I_+ < 5$); number represents distance (cm) from jet exit. [c] Species injected 20 cm from jet exit ($T \simeq 2000$ K). [d] Mass flux is of elemental metal only.

Table 2 Effect of hydrogen on electron attachment efficiency of SF_6 (injection at 20 cm; $T \simeq$ 2000 K) and WF_6 (injection at 11 cm; $T > 3000$ K)

Attacher	Mass flux (g/s)	Mass flux H_2 (g/s)	H/attacher molecule ratio	Electrostatic-probe data[a]
SF_6	10^{-3}	0	0	55P, 60P, 70F
SF_6	10^{-3}	4.7×10^{-5}	6	60P, 75F
SF_6	10^{-3}	2.1×10^{-3}	300	70N
WF_6	2.6×10^{-4}	0	0	16N, 20F
WF_6	2.6×10^{-4}	1.7×10^{-3}	2×10^{3}	16N, 20F
WF_6	2.6×10^{-4}	5×10^{-3}	5.7×10^{3}	30N, 40P, 50F
WF_6	2.6×10^{-4}	9×10^{-4}	1×10^{4}	30N, 40P, 50P, 60F
WF_6	2.6×10^{-4}	1.5×10^{-2}	1.7×10^{4}	60N, 70F

[a]Notations same as Table 1.

III. Attachment Data

The electrostatic-probe data are summarized in Table 1. Unless otherwise noted, attachers were injected at 11 cm from the jet exit at a local centerline temperature greater than 3000 K. In the last column, the number signifies distance in cm from the jet exit and the letters N, P, and F denote no attachment, partial attachment, and full attachment, respectively, at that point, as defined at the bottom of Table 1.

The table clearly shows that the most efficient attachers are WF_6 and MoF_6 and they are both superior to SF_6 at an injection temperature greater than 3000 K. The attachment efficiency of SF_6 is sensitive to the injection temperature: an order-of-magnitude higher mass flux is required to attach at a fixed axial location when injection is at 3000 K compared to injection at 2000 K. WF_6, on the other hand, appears to have an attachment efficiency that is insensitive to such temperature differences. Attachment is actually obtained farther downstream when WF_6 is injected at 20 cm (2000 K), due to the finite mixing rate between the attacher and the jet fluid.

The effect of hydrogen in the jet flow on attacher performance was investigated experimentally. Measured flow rates of hydrogen were added to the jet in a plenum upstream of the jet exit. The results of these experiments for SF_6 and WF_6 are summarized in Table 2. The performance of both species is degraded but the effect is more drastic for SF_6.

IV. Analysis

A. CMEF Centerline Properties

Measurements in the CMEF jet give values for the jet radius r, temperature T, and flow speed u. At the start of the jet inside the potential core, the physical conditions are $r_j = 1.3$ cm, $T_j = 3800$ K, and $u_j = 8\times10^4$ cm/s. Beyond this region, analytic fits to the measured properties are given by

$$r = 0.22\,(x-9) \quad \text{cm} \tag{1}$$

$$T = 300 + 2\times10^4/(x-9) \quad \text{K} \tag{2}$$

$$u = 3.5\times10^5/(x-9) \quad \text{cm/s} \tag{3}$$

where the distance x is given in cm and T and u are axis values.

The electron density in the jet decreases with distance because of dilution by entrained air and the dissociative neutralization reaction $NO^+ + e \rightarrow N + O$. As shown in Fig. 3, electrostatic-probe data and calculation are in very good agreement.

Oxygen-atom density, which starts at equilibrium at the jet-exit temperature and ambient pressure, also decreases because of dilution. Three-body recombination is not important because the rate constant is small ($k \approx 2\times10^{-32}/\sqrt{T}\,\text{cm}^6/\text{s}$).

B. Partial Equilibrium Limit

To qualify as fully attached, it is necessary that the electron density be reduced by a factor of 50 or more as compared to the local positive ion density. Using the equilibrium for the overall attachment reaction $A + e \rightleftharpoons A-$, we obtain the relation between the electron affinity, the local gas temperature, and the amount of attacher to give this ratio of electron to negative-ion density. This equilibrium is determined by

$$\frac{[e]\,[A]}{[A^-]} \approx (2\pi mkT/h^2)^{3/2} e^{-EA/kT} \tag{4}$$

where the right-hand side represents the equilibrium constant and the symbols have their usual meaning. In terms of the flux of particles added and taking account of dilution, the number density of attachers is given by

$$[A] = \frac{\dot{N}_{A_i}}{\pi r^2 u} \approx \frac{\dot{N}_{A_i}}{\pi r^2{}_j u_j}\,\frac{7.6}{(x-q)} \tag{5}$$

where $\dot{N}_{A_i}$ is the initial attacher flux. Combining Eqs. (4) and (5), we have the condition for attachment

$$0.02 = \frac{130 \quad (x-9)}{(\dot{N}_{A_i}/10^{18})}\, T^{3/2} e^{-EA/kT} \tag{6}$$

C. Attachment Rate

To estimate the attachment limit because of the attachment rate, we consider the rate of loss of electrons because of attachment, which is given by

$$\frac{dn_e}{dt} = -k_a n_e [A] \tag{7}$$

For full attachment, the electron density must drop to a value such that the ratio of positive ions to electrons is greater than or about 50. Changes of electron density by other means such as dilution, which change electron and ion densities in the same way, leaving the ratio of electron to ion densities unchanged. The rate constant k_a has a slight temperature dependence which we will neglect at this stage. Taking account of the dilution of the attacher for the jet growth, Eq. (5), and noting that before attachment starts the ion density is equal to the free-electron density, we integrate Eq. (7) and obtain an equation which relates the attachment-rate constant and the full attachment distance (x_a), x_i being the injection distance:

$$k_a = 8\times10^{10}/N_{A_i}\,(x_a - x_i) \tag{8}$$

D. Temperature Fluctuations

The partial equilibrium limit is sensitive to temperature [see Eq. (6)]. As a result, it is important to take account of temperature fluctuations because the regions above the average temperature will have much larger electron density and will increase the electron density above that calculated using the average temperature. We estimate this effect by assuming a Gaussian temperature distribution:

$$P(T) = B \exp[-(T-T_l)^2/2C^2(T_a-T_f)^2] \tag{9}$$

where the variable temperature T is limited to the range of the upper-limit temperature of the potential core of the jet and a lower-limit front temperature (T_f), taken to be equal to the ambient temperature. The normalization constant B is determined so that

$$\int_{T_{\min}}^{T_{\max}} P \mathrm{d}T = 1 \tag{10}$$

T_a is the axis temperature and $C=0.4$ is a coefficient determining the amplitude of the fluctuations which, in the wake studies of Sutton and Camac,[13] had a range 0.3-0.5, and was considered by these authors to be a reasonable range for turbulent flows. The constant T_l is determined so that

$$\int_{T_{\min}}^{T_{\max}} PT \mathrm{d}T = T_a \tag{11}$$

E. Turbulent Mixing

For attachment, the added material must be mixed molecularly with the electrons. As the eddies churn and break up, the electrons in the small eddies can be mixed by molecular diffusion and attached. We are concerned with residual fraction which may remain too large to be molecularly mixed. We assume that the residual volume is reduced exponentially according to

$$\frac{V}{V_i} \simeq \exp\left(-\int \frac{\mathrm{d}x}{u\tau}\right) \simeq \left(\frac{x_i}{x}\right)^4 \tag{12}$$

where u is the flow velocity, $\tau \approx l/u'$ is the eddy-turnover time, u' is the eddy velocity, l is the eddy macroscale, and we have used from Tennekes and Lumley[14]

$$(u'/u)^2 \approx l/x \tag{13}$$

and

$$l \approx 0.067x \tag{14}$$

Equation (12) overestimates the incomplete mixing when the largest eddies which started at the injection location have been reduced to a size where molecular diffusion can no longer be neglected. The largest eddy size is estimated as starting with a radius of about 1/5 of the jet radius and decreasing in size by about a factor of 2 with each turnover distance. The distance that material will diffuse in the time between eddy breakups for the pressure of 20 Torr is about 0.12 cm. Thus, mixing should occur in a distance comparable with the injection distance because this corresponds to four turnover distances.

F. Map for Attachment Analysis

In order to aid in the CMEF attachment analysis, we have organized the material given in the previous sections in a correlation map of the key phenomenology (Fig. 6). The map contains curves corresponding to attachment limits because of partial equilibrium and the attachment rate. The ordinate of the map is the injected flux of attacher particles and the abscissa is the distance along the axis of the CMEF.

The partial equilibrium attachment locations for electron-attachment energy are indicated by almost vertical lines in the figure. The lines are almost vertical since they are not sensitive to the particle flux. They are, however, sensitive to temperature so that as the electron affinity drops, the distance to this attachment limit increases. At lower particle fluxes, the

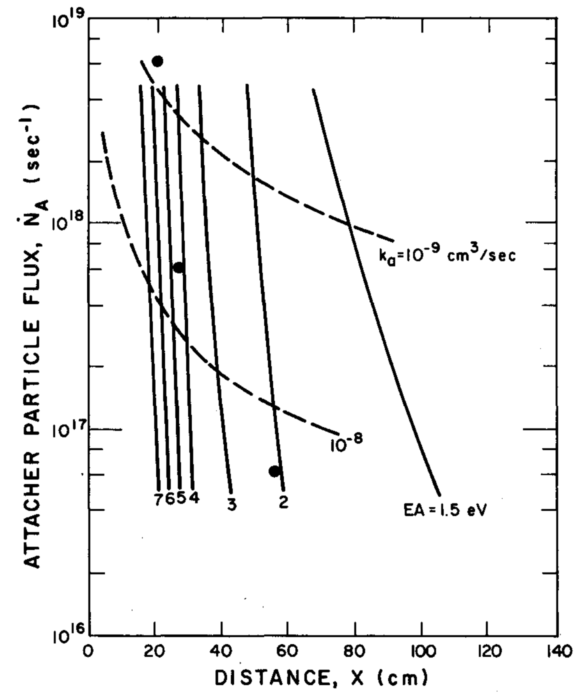

Fig. 6 Location of attachment plotted as attacher-particle flux vs axial distance in CMEF. Points indicate measured attachment for WF_6 injection at T > 3000 K.

distances are somewhat longer, implying that slightly lower temperatures will be required to reduce the electron density to the attachment criterion. The curves labeled k_a are for the attachment-rate limit. When the product $k_a[A]$ is large, the attachment occurs rapidly and goes asymptotically to the injection location of 11 cm. When the product $k_a[A]$ is small, the attachment distance increases, inversely proportional to $k_a[A]$. Thus, for a given attacher flux, both k_a (and the corresponding dashed curve) and EA (and the corresponding solid curve) determine attachment distances. It is the longer of these two values which will be the actual attachment location.

G. Other Effects

There are a number of thermal and chemical effects which modify the interpretation of the attachment analysis obtained from the map just described. These include: 1) thermal destruction, 2) chemical destruction, 3) thermal transformation, 4) chemical transformation, 5) chemi-detachment, 6) chemical changes which favor the attachment direction of the partial equilibrium, and 7) chemical cooling. Some of these act to improve the effectiveness of the attacher, while others have the opposite effect. In general, they do not change the form of the attachment map which has regions limited by partial equilibrium and regions limited by the attachment rate.

H. Tungsten Oxides

Tungsten rods, water-cooled tubes, and powder have been used in the CMEF. The shortest attachment distance was observed at 29 cm when injection was at 7 cm. The injected mass flux is about 1.2×10^{-3} g/s which, if all WO_3, corresponds to a molecule flux of 3×10^{18} s^{-1}. From this mass flux we estimate the electron affinity to be about 3.6 eV, in agreement with results from analysis of flame data by Jensen and Miller.[15] We estimate the attachment-rate constant from lower mass-flux CMEF data using WO_3 powder. With a powder mass flux of 2×10^{-4} g/s, attachment was observed at 65 cm. This corresponds to an attachment-rate constant $k_a \gtrsim 3\times10^{-9}$ cm^3/s if all the attaching molecules are WO_3; the rate constant becomes 6×10^{-9} cm^3/s if all the

Table 3 Hexafluoride electron-affinity and dissociation-energy values

Element X	Z	Electron affinity XF_6^- (eV) Ref. 20	Ref. 21	Ref. 23	Refs. 16,17	Ref. 18	Dissociation energy $XF_5 - F$ (eV)
S	16	0.6 ± 0.1	0.7		0.46		3.3[2] 4.0[24]
Se	34	3.0 ± 0.2	2.9		2.9		
Mo	42				>5.1	≥ 4.5	4.1[25]
Te	52	3.2 ± 0.2	2.6		3.3		
W	74	4.5 ± 0.2			≥ 5.1	≥ 4.9	5.26[22]
Re	75				>5.1		
Pt	78	$6.8 \geq 1$			>5.1		
U	92	$4.9 \geq 0.5$	5.0	≥ 5.1		≥ 4.3	3.0[26]

attaching molecules are W_2O_6, and so on. The data we have are not enough to determine the relative distribution of the various tungsten oxides.

I. Hexafluorides

For WF_6, the electron affinity is estimated to be 5.5 eV from Fig. 6; this agrees very well with recent measurements reported in the literature.[16-18] The attachment rate is estimated to be 3×10^{-8} cm^3/s.

The electron affinity in hexaflourides appears to increase with molecular weight.[19-21] Physically, this is related to the atomic size of the core atom. Theoretical and experimental values of electron affinities from current literature are given in Table 3, which also lists some values for the dissociation energy. From the limited data, it appears that UF_6 is comparable to SF_6 and should be similar in regard to thermal breakup.

V. Conclusions

Sulfur hexaflouride is an excellent electron attacher at room temperature because it has a very large attachment-rate constant ($\approx 2 \times 10^{-7}$ cm^3/s). As the temperature increases, however, other properties of the attaching molecule become increasingly more important. In fact, SF_6 becomes a poor electron attacher when the temperature exceeds about 2000 K. A more general set of the important characteristics required for good electron attachers should include at least the following: 1) large attachment-rate constant, 2) thermal and chemical stability, and 3) large electron affinity-negative-ion stability.

The requirement for a large attachment-rate constant is obvious; it enables electron attachment to occur within a sufficiently short time and with the addition of an acceptably small amount of the attacher. Results of our analyses and attachment measurement on a large number of candidate attacher molecules indicate that many of these molecules have attachment-rate constants larger than 10^{-8} cm^3/s, and should be adequate for most practical applications.

For high-temperature applications, thermal- and chemical-stability considerations become more important because most molecules decompose faster and are more reactive at higher temperatures. This degradation of attachment performance is demonstrated by the CMEF data for several attachers, including SF_6.

Reactions with other molecules present in the environment may also seriously degrade attachment performance, especially at high temperatures; oxidation and hydrogenation are two important examples. CMEF data show that hydrogen, when present in high enough concentrations, degrades the high-temperature attachment performance of SF_6 and WF_6.

The electron-attachment process removes electrons by forming negative ions. At the same time, however, electrons are produced from negative ions by the detachment process. The stability of a negative ion is a strong function of the electron affinity. We have shown that large electron affinities are necessary to achieve attachment at high temperatures. CMEF data also indicate that tungsten oxides have an electron affinity of about 3.6 eV and tungsten hexaflouride, the best high-temperature electron attacher among all the candidates investigated, has an electron affinity greater that 5 eV.

Acknowledgments

The authors are indebted to L.P. Ruotolo for his assistance in carrying out the experiments. This work was supported by the Space and Missile Systems Organization, Air Force Systems Command.

References

[1] Fehsenfeld, F. C., "Electron Attachment to SF_6," *Journal of Chemical Physics*, Vol. 53, Sept. 1, 1970, pp. 2000-2004.

[2] Bott, J. F. and Jacobs, T. A., "Shock-Tube Studies of Sulfur Hexafluoride," *Journal of Chemical Physics*, Vol. 50, May 1, 1969, pp. 3850-3855.

[3] Modica, A., Stepakoff, G., and Rosenbaum, H., "A Shock-Tube Study of Plasma Alleviation by Oxide Dust," *Ninth International Shock Tube Symposium*, 1973, pp. 227-237.

[4] Schroeder, L. C. and Akey, N. D., "Material-Injection Alleviation During the RAM C-III Flight," *Journal of Spacecraft and Rockets*, Vol. 10, March 1973, pp. 170-174.

[5] Gould, R. K. and Miller, W. J., "Electron Attachment and Compound Formation in Flames VI Negative Ion and Compound Formation in Flames Containing Rhenium and Potassium," *Journal of Chemical Physics*, Vol. 62, Jan. 15, 1975, pp. 644-649.

[6] Mandl, A., Fogelson, S. A., and Hester, S. D., "The Chemical Modeling Experimental Facility," *AIAA Journal*, Vol. 11, Dec. 1973, pp. 1711-1714.

[7] Mott-Smith, H. M. and Langmuir, I., "The Theory of Collectors in Gaseous Discharges," *Physical Review*, Vol. 28, Oct. 1926, pp. 727-763.

[8] Laframboise, J., "Theory of Cylindrical and Spherical Langmuir Probes in a Collisionless Plasma at Rest," *Rarefied Gas Dynamics*, Vol. 2, 1966, pp. 22-44.

[9] Zakharova, V. M., Kgan, Y. M., Mustafin, K. S., and Perel, V. I., "Probe Measurements at Medium Pressures," *Soviet Physics-Technical Physics*, Vol. 5, April 1960, pp. 411-419. [*Zhurnal Tekhnicheskoi Fiziki*, Vol. 30, April 1960, pp. 442-449.]

[10] Kiel, R. E., "Continuum Electrostatic-Probe Theory for Large Sheaths on Spheres and Cylinders," *Journal of Applied Physics*, Vol. 40, Aug. 1969, pp. 3668-3673.

[11] Scharfman, W. E. and Taylor, W. C., "Studies of Convective Effects on the Operation of Continuum Electrostatic Probes," *Stanford Research Institute Report*, Project 7712, Menlo Park, Calif., April 1971.

[12] Chung, P. M., Talbot, L., and Touryan, K. J., *Electric Probes in Stationary and Flowing Plasmas: Theory and Application*. Springer-Verlag, New York, 1975, pp. 27ff and pp. 47ff.

[13] Sutton, G. W. and Camac, M., "Wake-Temperature Turbulent Fluctuation Decay Rates Deduced from O_2 Radiation," *AIAA Journal*, Vol. 6, Dec. 1968, pp. 2402-2410.

[14] Tennekes, H. and Lumley, J. L., *A First Course in Turbulence*, MIT Press, Cambridge, Mass., 1972.

[15] Jensen, D. E. and Miller, W. J., "Electron Attachment and Compound Formation in Flames. III. Negative Ion and Compound

Formation in Flames Containing Tungsten and Potassium," *Journal of Chemical Physics*, Vol. 53, Oct. 15, 1970, pp. 3287-3292.

[16]Compton, R. N., Reinhardt, P. W., and Cooper, C. D., "Collisional Ionization between Fast Alkali Atoms and Selected Hexafluoride Molecules," *Journal of Chemical Physics*, Vol. 68, March 1, 1978, pp. 2023-2036.

[17]Burgess, J., Haigh, I., Peacock, R. D., and Taylor, P. J., *Chemical Society Dalton Transactions*, 1974, p. 1064.

[18]Mathur, B. P., Rothe, E. W., and Reck, G. P., "Ionization Reactions of Metal Hexafluorides with Alkali Atoms and Dimers," *Journal of Chemical Physics*, Vol. 67, July 15, 1977, pp. 377-381.

[19]Bartlett, N., "The Oxidizing Properties of the Third Transition Series Hexafluorides and Related Compounds," *Angewandte Chemie, International Edition in English*, Vol. 7, June 1968, pp. 433-439.

[20]Beauchamp, J. L., "Ion Cyclotron Resonance Studies of Endothermic Reactions of UF_6^- Generated by Surface Ionization," *Journal of Chemical Physics*, Vol. 64, Feb. 1, 1976, pp. 929-935.

[21]Boring, M., "Calculated Electron Affinities of a Selected Series of Hexafluorides," *Chemical Physics Letters*, Vol. 46, March 1, 1977, pp. 242-244.

[22]Hildenbrand, D. L., "Thermochemistry of the Gaseous Tungsten Fluorides," *Journal of Chemical Physics*, Vol. 62, April 15, 1975, pp. 3074-3079.

[23]Compton, R. N., "On the Formation of Positive and Negative Ions in Gaseous UF_6," *Journal of Chemical Physics*, Vol. 66, May 15, 1977, pp. 4478-4485.

[24]Benson, S. W., "Thermochemistry and Kinetics of Sulfur-Containing Molecules and Radicals," *Chemical Reviews*, Vol. 78, Feb. 1978, pp. 23-35.

[25]Hildenbrand, D. L., "Thermochemical Studies of the Gaseous Lower-Valent Fluorides of Molybdenum," *Journal of Chemical Physics*, Vol. 65, July 15, 1976, pp. 614-618.

[26]Hildenbrand, D. L., "Thermochemistry of Gaseous UF_5 and UF_4," *Journal of Chemical Physics*, Vol. 66, June 1, 1977, pp. 4788-4794.